Remote Sensing of Environment 124 (2012) 466–478

Contents lists available at SciVerse ScienceDirect

Remote Sensing of Environment

journal homepage: www.elsevier.com/locate/rse

Mapping forest aboveground biomass in the Northeastern United States with ALOS PALSAR dual-polarization L-band

Oliver Cartus [a,*], Maurizio Santoro [b], Josef Kellndorfer [c]

[a] Woods Hole Research Center, 149 Woods Hole Road, Falmouth, MA 02540-1644, USA
[b] Gamma Remote Sensing, 3073 Gümligen, Switzerland
[c] Woods Hole Research Center, Falmouth, MA 02540-1644, USA

ARTICLE INFO

Article history:
Received 17 October 2011
Received in revised form 22 May 2012
Accepted 26 May 2012
Available online 4 July 2012

Keywords:
ALOS PALSAR
Dual-polarization intensity
Aboveground biomass
Northeastern United States
NBCD
Synergy

ABSTRACT

A method for regional scale mapping of aboveground forest biomass with Advanced Land Observing Satellite (ALOS) Phased Array type L-band Synthetic Aperture Radar (PALSAR) data is presented. A fully automated algorithm, exploiting the synergy of SAR and optical remote sensing for the calibration of a semi-empirical model (Santoro et al., 2011; Cartus et al., 2011), was adopted to map forest aboveground biomass with L-band HH and HV intensity in the northeastern United States. In the retrieval algorithm, a semi-empirical model is calibrated and inverted for each HH and HV image to estimate biomass at the pixel level. Where possible, biomass estimates for single images in a multi-temporal stack were combined in a weighted manner. A comparison with the National Biomass and Carbon Dataset, NBCD 2000 (Kellndorfer et al., in preparation), at different spatial scales indicated the feasibility of the automated biomass retrieval approach and confirmed previous findings that the retrieval accuracy for HV intensity is consistently better than that for HH intensity and depends on the imaging conditions. The weighted combination of the biomass estimates from each intensity image in a multi-temporal stack significantly improved the retrieval performance. Because of regional differences in the multi-temporal coverage with ALOS PALSAR dual polarization data (1–5 images for 2007/08) and the pronounced dependence of the retrieval for single images on the imaging conditions, the possibility of producing maps with consistent accuracy at high resolution was found to be limited. Accurate biomass estimates were obtained when aggregating the ALOS biomass maps at county scale and comparing the estimates to Forest Inventory and Analysis (FIA) county statistics (RMSE = 12.9 t/ha, $R^2 = 0.86$).

1. Introduction

The spatially explicit quantification of the world's forest resources in terms of key biophysical parameters such as growing stock volume (i.e., the volume of stems per unit area) or aboveground biomass (i.e., the dry weight of organic matter present in stems, bark and branches per unit area) has been a long-standing goal in the remote sensing community since these parameters are closely related to the amount of carbon that is stored in forest vegetation and thus key to our understanding of the terrestrial carbon balance (Houghton, 2005). Meanwhile, a wide range of methods that integrate remote sensing data in various ways have been developed to map growing stock volume and aboveground biomass at regional to global scales. A rather simple approach, referred to as "Stratify and Multiply" in Goetz et al. (2009), utilizes land cover maps derived from medium to low resolution optical remote sensing data to stratify forest vegetation and to extrapolate biome default values of growing stock volume or biomass (e.g., Ruesch and Gibbs, 2008). Another common approach utilizes National Forest Inventory data (NFI) or ancillary *in situ* measurements for the development of models relating reflectance values in different spectral bands or band ratios like the Normalized Difference Vegetation Index (NDVI) to the forest biophysical parameters in order to produce regional to continental scale maps (Baccini et al., 2008; Blackard et al., 2008; Myneni et al., 2001; Reese et al., 2003; Tomppo et al., 2008). In recent years, Light Detection and Ranging (Lidar) has also shown great potential for the retrieval of forest biophysical parameters. Wall-to-wall coverage of large areas with Lidar is, however, impractical, which is why optical remote sensing data or derived map products are used to extrapolate the estimates for Lidar samples to large areas (Boudreau et al., 2008; Lefsky, 2010; Nelson et al., 2009).

In the case of spaceborne Synthetic Aperture Radar (SAR), regional growing stock volume or aboveground biomass products have so far been developed based on Shuttle Radar and Topography Mission (SRTM) C-band (~5 cm wavelength) interferometric data for the conterminous United States (Kellndorfer et al., 2006; Kellndorfer et al., in preparation), based on ERS-1/2 C-band repeat-pass coherence for Central Siberia and Northeast China (Cartus et al., 2011; Wagner et

* Corresponding author. Tel.: +1 508 444 1573; fax: +1 508 540 9700.
E-mail address: ocartus@whrc.org (O. Cartus).

0034-4257/$ – see front matter © 2012 Elsevier Inc. All rights reserved.
doi:10.1016/j.rse.2012.05.029

al., 2003) and based on multi-temporal stacks of C-band intensity acquired by ENVISAT ASAR in ScanSAR mode for Sweden and Central Siberia (Santoro et al., 2011). Applications of longer wavelength L-band (~23 cm wavelength), which has been available through a series of shuttle and satellite missions (SEASAT, the Shuttle Imaging Radar, SIR-C, the Japanese Earth Resources Satellite, JERS, and the Advanced Land Observing Satellite Phased Array type L-band Synthetic Aperture Radar, ALOS PALSAR), have been scarce. In Saatchi et al. (2007), co-polarized L-band backscatter intensity from JERS was used to estimate the biomass of savanna, disturbed and secondary forests and tree plantations in the Amazon basin. Various authors have investigated the use of L-band intensity for the retrieval of growing stock volume or aboveground biomass at selected test sites. Most studies report high temporal consistency (Askne et al., 2003; Baker and Luckman, 1999; Harrell et al., 1995; Sandberg et al., 2011; Santoro et al., 2006, 2009) and superior sensitivity of L-band to forest biophysical parameters compared to shorter wavelength radars because of its increased ability to penetrate forest canopies (Castel et al., 2001; Dobson et al., 1992; Fransson and Israelsson, 1999; Harrell et al., 1997; Hoekman and Quinones, 2000; Hyyppä et al., 2000; Saatchi and Moghaddam, 2000; Sandberg et al., 2011). The highest sensitivity to growing stock volume or aboveground biomass was reported for L-band intensity in cross-polarization (Balzter et al., 2002; Castel et al., 2001; Dobson et al., 1992; Harrell et al., 1997; Hoekman and Quinones, 2000; Kellndorfer et al., 2003; Le Toan et al., 1992; Ranson and Sun, 1994, 2000). Investigations on the use of spaceborne interferometric L-band for forest mapping (i.e., repeat-pass coherence or phase) were less promising; mostly due to the long repeat cycles of the hitherto spaceborne missions resulting in strong temporal decorrelation with some exceptions only for image pairs that were acquired under long term stable conditions (Thiel et al., 2009). Investigations of airborne data, however, have indicated the great potential of interferometric fully-polarimetric L-band for the mapping of forest canopy height when the time span between the acquisitions of the interferometric image pairs is short and the baseline in a suitable range (Hajnsek et al., 2009; Neumann et al., 2010; Papathanassiou and Cloude, 2001).

L-band backscatter from forested terrain consists primarily of volume backscatter from the forest canopies (Chauhan et al., 1991; Karam et al., 1995; Skriver et al., 1994; Way et al., 1994) and surface backscatter from the forest floor when there are gaps in the canopy. Although the L-band signal penetrates even dense tropical forests (Hajnsek et al., 2009), the contribution of stem–ground interactions to the total backscatter is supposed to be relatively weak due to diffuse scattering at the rough forest floor and substantial attenuation of the signals in the vegetation layer (Dobson et al., 1992; Pulliainen et al., 1999). Still, relevant contributions of stem–ground interactions to the total backscatter from forest have been reported for HH polarization, e.g. under frozen conditions when the canopies become more transparent to the radar signal (Way et al., 1994). All investigations reported an increase of L-band backscatter with increasing forest growing stock volume or aboveground biomass as with increasing canopy density and height, the backscatter contribution from the forest floor declines and the volume scattering contribution from the canopy increases. Saturation (i.e., the level beyond which the measurements no longer show any sensitivity to biomass) depends on the forest structure and has been reported to occur in biomass ranges of 80 to 150 t/ha for savanna (Lucas et al., 2006, 2010; Mitchard et al., 2009), 40 to 150 t/ha for boreal and temperate forests (Dobson et al., 1992; Imhoff, 1995; Le Toan et al., 1992; Ranson and Sun, 1994; Ranson et al., 1995; Sandberg et al., 2011) and 40 to 150 t/ha in the tropics (Imhoff, 1995; Luckman et al., 1997; Saatchi et al., 2011). L-band backscatter from forested terrain was observed to depend on the imaging conditions, in particular the wet/dry or frozen/unfrozen state of the soils and vegetation or, if present, the properties of the snow cover (Askne et al., 2003; Harrell et al., 1995; Kasischke et al., 2011; Kwok et al., 1994; Lucas et al., 2010; Pierce et al., 1998; Pulliainen et al., 1999; Ranson and Sun, 2000; Ranson et al., 1995; Rignot et al., 1994a, 1994b; Saatchi and Moghaddam, 2000; Salas et al., 2002; Sandberg et al., 2011; Santoro et al., 2006; Way et al., 1994). The imaging conditions affect 1) the overall backscatter strength from the forest floor and the canopy and 2) the sensitivity to forest biophysical parameters (Harrell et al., 1995, 1997; Pulliainen et al., 1999; Ranson and Sun, 2000; Rauste, 2005; Rignot et al., 1994a; Santoro et al., 2006). In order to capture the contribution of the environmental conditions to the measured forest backscatter, the retrieval of growing stock volume or aboveground biomass with L-band intensity thus requires a set of *in situ* measurements to tune models that relate the measured backscatter to the biophysical forest parameters to the prevailing conditions. Extensive *in situ* data are often not available, either because of the vastness or remoteness of forests or because of restrictions on the use of existing measurements (e.g., from NFI). Even if available, uncertainties connected to *in situ* measurements can be substantial (e.g., Saatchi and Moghaddam, 2000). A fully automated algorithm that makes the retrieval independent of in situ data was recently presented in Santoro et al. (2011) for multi-temporal ENVISAT ASAR ScanSAR C-band data to map boreal forest growing stock volume. A similar approach was presented in Cartus et al. (2011) for ERS-1/2 tandem coherence to map growing stock volume classes in Northeast China. In both studies, the automation of the retrieval was accomplished with the aid of the MODIS Vegetation Continuous Field product, VCF (Hansen et al., 2003), which was used to calibrate semi-empirical models, relating the SAR/InSAR data to growing stock volume.

Between its launch in January 2006 and its failure in April 2011, ALOS PALSAR has acquired wall-to-wall global coverage in Fine-Beam dual-polarization mode (FBD) on an annual basis, which has resulted in up to five acquisitions per year at a particular location (Rosenqvist et al., 2007). The scope of the work presented in this paper was to investigate options for the exploitation of this extensive L-band database for large-area mapping of aboveground biomass. In this paper, we present a retrieval approach to regional scale mapping of aboveground biomass with ALOS PALSAR dual polarization data. The deployment of a retrieval algorithm required investigations of:

- the modeling of L-band backscatter in co- and cross-polarization as function of aboveground biomass using a semi-empirical approach
- the feasibility of an automated model training approach, similar to those presented in Santoro et al. (2011) and Cartus et al. (2011)
- the retrieval performance at different spatial scales, considering the influence of the imaging conditions and the benefit of having multi-temporal data stacks

The area of focus for this study was the northeastern United States for which a multi-temporal FBD dataset was acquired for the 2007/08 time period. The National Biomass and Carbon Dataset 2000 (Kellndorfer et al., in preparation) and USDA Forest and Inventory Analysis county-level statistics were used for comparison. The ALOS PALSAR and ancillary datasets are described in Section 2. In Section 3, the retrieval algorithm is described, which comprises a description of the semi-empirical model that was used to relate L-band backscatter to aboveground biomass as well as the model training and the inversion procedure. In Sections 4 and 5, the performance of the retrieval algorithm is discussed.

2. Study area and data

2.1. Study area

The retrieval of aboveground biomass with ALOS PALSAR data was tested for the northeastern United States (67–82°W, 37–47.5°N, see Fig. 1). According to the division of forest ecosystem provinces established by the US Forest Service (Bailey, 1995), the forests in the Northeast belong to the Laurentian Mixed Forest and Eastern

Broadleaf Forest Provinces (incl. associated mountain provinces). The Laurentian Mixed Forest Province comprises transitional forests between the boreal forests in the north and the temperate forests further south. This province consists of mixed (*Pinus*, *Betula*, *Acer* and *Fagus* species), pure coniferous (*Picea, Abies* species) or hardwood forests. In the mountainous areas between northern New York and Maine, hardwood forests can be found in valleys (*Acer*, *Betula* and *Fagus* species) and mixed forests (*Picea*, *Abies*, *Acer*, *Fagus* and *Betula* species) at lower altitude slopes. The forests at higher altitudes are dominated by coniferous species (*Abies, Pinus*). The Eastern Broadleaf Forest Province in the coastal regions between New Jersey and southern Maine hosts temperate deciduous forests with a large diversity of species on moist well-drained sites (e.g., *Fagus*, *Tilia*, *Liriodendron*, *Acer*, *Aesculus*, *Quercus*) and *Pinus-Quercus* forests on dry sandy soils. Further east in the Appalachian Mountains, the altitude influences the species composition with lower altitudes dominated by hardwood forests and higher altitudes dominated by conifers.

2.2. Data

2.2.1. ALOS PALSAR data

655 ALOS PALSAR Fine Beam Dual Polarization (FBD) scenes were obtained from the Alaska Satellite Facility (ASF). The FBD images were acquired with an off-nadir angle of 34.3° (incidence angle between 36.6° and 40.9°) and covered an area of ~70×70 km^2 each. The majority of the images were acquired in 2007 and 2008 between May and October; note that the ALOS acquisition plan foresaw FBD data acquisition for ascending (nighttime) orbits throughout the summer season (Rosenqvist et al., 2007). Pre-processing of the single-look complex (SLC) data included absolute calibration (Shimada et al., 2009), 2×8 multi-looking in range and azimuth, GAMMA MAP speckle filtering (Lopes et al., 1993) and terrain-corrected geocoding with the aid of the ALOS orbit data as well as the SRTM 1-arcsec Digital Elevation Model (DEM). The geocoded images were re-sampled to a regular grid with 30×30 m^2 pixel size. In order to account for topographic effects, the pre-processing included 1) compensation for topographic alterations of the pixel area contributing to the total backscatter (Holecz et al., 1994) and 2) normalization with respect to the dependence of surface and volume scattering on the local incidence angle. The dependence of these scattering mechanisms on the local incidence angle was compensated for with (Castel et al., 2001):

$$\sigma^0_{\text{norm}} = \sigma^0(\theta_i)\left(\frac{\cos(\theta)}{\cos(\theta_i^{\,i})}\right) \tag{1}$$

with θ being the incidence angle and θ_i the local incidence angle. Fig. 1 shows a mosaic of the terrain-corrected, geocoded and normalized FBD images. The figure also illustrates for part of the area how many images were available at a particular location.

2.2.2. USDA Forest Inventory and Analysis

Plot measurements and derived estimates of the major forest attributes were available from the US Forest Service Forest Inventory and Analysis (FIA) plot network ("http://fia.fs.fed.us/"). Since 1998, inventory measurements for plots with a standardized design (four subplots with 24 ft/7.3 m radius) were carried out annually for approximately 20% of plots per state. The sampling density was approximately 1 plot per 6000 acres (~2400 ha). The FIA database version 4 includes aboveground biomass estimates, which were obtained by means of allometric relations (Jenkins et al., 2003). The database also provides plot location information; however, for legal reasons these coordinates are fuzzed (i.e., actual plot locations could be up to one mile from the specified location) and for 20% of the plots in each county the plot coordinates have been swapped. Hence, it was not possible to directly link the plot and remote sensing data. Nevertheless, the FIA database was useful in this study for the characterization of the distribution of biomass in the study area. Only plots that were surveyed after the year 2000 were considered. In addition, ca. 2007 county-level total aboveground biomass statistics for 143 counties in Maine, Massachusetts, New Hampshire, Vermont, Rhode Island, Connecticut, New York and New Jersey were obtained via the EVALIDator online inventory tool of the US Forest Service ("http://fiatools.fs.fed.us"). The county-level statistics were derived from FIA plot data using remote sensing imagery (aerial photos or Landsat imagery) that was classified to forest/non-forest classes for the stratification of the sample plots to estimate the average or total biomass per stratum. For a detailed description of how the county-level statistics were derived, the reader is referred to Bechtold and Patterson (2005).

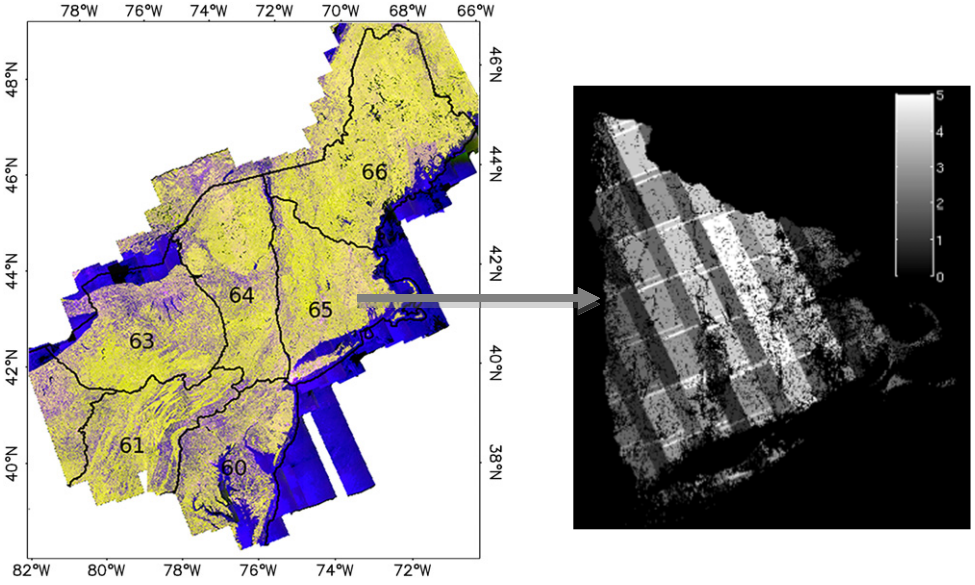

Fig. 1. RGB mosaic of ALOS PALSAR FBD data for the northeastern US and the extent of the mapping zones 60 to 66. The red channel shows the HH intensity, the green channel the HV intensity and the blue channel the HH/HV ratio. The image on the right-hand side illustrates for the forest areas in zone 65 the number of FBD acquisitions.

2.2.3. National Biomass and Carbon Dataset 2000

Since the FIA plot data could not be linked to the ALOS data and other spatially explicit in situ measurements were not available, the National Biomass and Carbon Dataset 2000 (NBCD), providing estimates of canopy height and aboveground biomass at 30 m pixel size for the conterminous United States, was considered for comparison (Kellndorfer et al., 2006, in preparation). For the production of the NBCD map, FIA plot data were used as a reference to develop ensemble regression tree models using Landsat ETM + data, national Landsat-based maps of canopy density and land cover (see Section 2.2.4) as well as the 1 arc sec USGS National Elevation Data (NED, Gesch et al., 2002) and interferometric C-band SRTM DEMs as spatial predictor layers. Differentiation of NED and SRTM elevations, which in the case of forest represent the ground elevation plus the height of the scattering phase center within the canopy, allowed the estimation of the height of the scattering phase center relative to the ground surface (Kellndorfer et al., 2004; Walker et al., 2007). The training of regression tree models that related the spatial predictors such as the scattering phase center height (SRTM/NED), canopy density (NLCD) or the Landsat spectral data to canopy height and biomass, was carried out at object level (i.e., the image data were segmented to mitigate the effect of noise in the predictor layers); note that in the case of the NBCD analysis the US Forest Service linked the FIA survey data to the corresponding image segments, i.e., FIA plot locations were not released. Models were developed for 66 eco-floristic zones spanning the conterminous United States; the zonal boundaries were adapted from the NLCD project (see Section 2.2.4). The models were used to produce forest canopy height and aboveground biomass maps at 30 m postings for each of the 66 mapping zones. The results of a bootstrap validation against FIA plot estimates of aboveground biomass for six mapping zones in the northeastern United States have been summarized in Table 1 (Kellndorfer et al., in preparation). The validation of the NBCD map showed no bias with respect to the FIA survey data and no sign of saturation in the estimates for aboveground biomass in the northeastern United States. An additional comparison of the NBCD biomass estimates with FIA county-level statistics resulted in an RMSE of 14 t/ha (for the entire conterminous US).

2.2.4. Optical remote sensing products

In Cartus et al. (2011) and Santoro et al. (2011), the MODIS VCF canopy cover product (Hansen et al., 2003), which provides global estimates of percent canopy cover at 500 m pixel size, was used to identify open ground and dense forest areas in SAR and InSAR imagery. For the United States, the Multi-Resolution Land Characteristics Consortium (MRLC) has released a high resolution Landsat-based National Land Cover Database (NLCD), which includes a national map of canopy density (CD) with a pixel size of 30 m (i.e., similar to that of the ALOS data). The CD map for 2001 was produced based on empirical regression tree models that were trained with the aid of 1 m ortho-imagery. The CD map reports canopy densities between 1% and 100% for trees at least 5 m tall; note that canopy density in contrast to canopy cover (VCF) does not consider gaps within the canopy. The error of the CD map was reported to be in a range of 6% to 17% (Homer et al., 2007). The NLCD database also includes nationwide 30 m maps of land cover (for 1992, 2001 and 2006). The land cover map for 2006 represents an updated version of the 2001 map. For the production of the land cover maps, Landsat data as well as ancillary datasets like DEM-based estimates of slope and aspect angle were used as input to a decision tree classifier. The training data included various data sources such as existing land cover maps, ortho-imagery, FIA or ancillary field data. Initial validation results for the 2001 map indicated an overall accuracy of 84% (Homer et al., 2007).

Table 1
FIA-based bootstrap validation results for the NBCD biomass map in the Northeastern USA. The table reports the root mean square error (RMSE) and the bias (Kellndorfer et al., in preparation).

Zone	RMSE [t/ha]	Bias [t/ha]
60	60	1.1
61	56	0.13
63	52	0.41
64	50	0.25
65	48	−0.02
66	42	−0.02

2.2.5. Weather data

Meteorological measurements from 64 weather stations located in New York State were obtained from the NOAA National Climatic Data Center for the year 2007. The weather data included daily summaries of temperature (minimum, average and maximum), precipitation and snow depth.

3. Method

3.1. Modeling

The goal of a robust and transferable retrieval algorithm advises the use of a physically-based approach for the modeling of backscatter as function of forest biophysical parameters. However, when aiming at retrieval the model formulation needs to be simple enough so that it can be inverted (i.e., the number of scattering mechanisms and influencing factors that can be considered is limited). A reasonable compromise between these opposing demands is generally represented by the Water–Cloud family of models (Attema and Ulaby, 1978). For the modeling of L-band backscatter, we have therefore considered a version of the Water–Cloud Model that has been extended to account for vertical and horizontal discontinuities (i.e., gaps) in the canopy (Askne et al., 1997). In the model, the backscatter from forest, σ^0_{for}, is considered a sum of three contributions:

$$\sigma^0_{\text{for}} = (1-\eta)\sigma^0_{\text{gr}} + \eta\sigma^0_{\text{gr}}e^{-\alpha h} + \eta\sigma^0_{\text{veg}}\left(1-e^{-\alpha h}\right) \quad (2)$$

The first term describes the direct backscatter from the forest floor, σ^0_{gr}, through gaps in the canopy. The parameter η represents the area-fill factor (i.e., the percentage to which the ground is covered by the canopy). In other words, η describes the canopy cover. The second term describes the backscatter from the ground that was attenuated in the canopy. Herein, the exponential represents the two-way tree transmissivity, which depends on the canopy height, h, and the two-way signal attenuation, α. The third term describes the volume backscatter, σ^0_{veg}, from an opaque canopy without gaps. The model in Eq. (2) can also be written in the following form:

$$\sigma^0_{\text{for}} = \sigma^0_{\text{gr}}T_{\text{for}} + \sigma^0_{\text{veg}}(1-T_{\text{for}}) \quad (3)$$

where T_{for} represents the forest transmissivity:

$$T_{\text{for}} = (1-\eta) + \eta e^{-\alpha h} \quad (4)$$

One of the underlying assumptions of Water–Cloud models is that higher order scattering can be neglected. We have already discussed above that under typical conditions (rough forest floor, substantial attenuation in the canopy) stem–ground interactions can be neglected in L-band (Dobson et al., 1992; Pulliainen et al., 1999). Significant contributions of higher order scattering may also arise from the canopies. A number of authors have modeled the effect of higher order scattering from forest canopies for co- and cross-polarization L-band. While all showed that higher order scattering effects were negligible in co-polarization, the results differed somewhat in the case of cross-polarization. In Wang et al. (1998), the consideration

of higher order scattering increased the modeled L-HV backscatter from pine forest for about 1.5 to 2 dB (at ~35° incidence angle). By contrast, Karam et al. (1992) noted that higher order scattering from walnut orchards had a significant effect at HV polarization only in X-band but not in L-band, regardless of the incidence angle. In a study of a forested site in France, Picard et al. (2004) observed an underestimation of L-HV backscatter as a function of growing stock volume for about 2 dB when only first order scattering in a model was considered. However, when multiple scattering effects were considered, the backscatter was overestimated by up to 2 dB compared to SIR-C L-HV measurements (at 26° and 54° incidence angle). Picard et al. concluded that the improvements in the modeling when considering multiple scattering effects were minor compared to the overall uncertainty in the modeling and that, in contrast to C-HV, the modeled relationship between L-HV backscatter and growing stock volume when considering only first order scattering depicted well the observed relationship of SIR-C L-HV intensity and growing stock volume.

The model in Eq. (2) expresses the forest backscatter as a function of the canopy height and the area-fill factor, which is an uncommon parameter in forest inventories. According to scatterometer experiments at X- and C-bands at boreal forest sites (Pulliainen et al., 1994), T_{for} can also be expressed as function of growing stock volume, GSV [m^3/ha]:

$$T_{for} = e^{-\beta GSV} \tag{5}$$

with β being an empirical parameter. Since, in this study, aboveground biomass was the observable and growing stock volume is commonly considered a proxy for biomass (i.e., aboveground biomass can be estimated from growing stock volume using age-dependent biomass expansion factors, e.g., IPCC, 2006), we replaced growing stock volume with aboveground biomass, B [t/ha], so that the forest backscatter could be modeled as function of biomass:

$$\sigma^0_{for} = \sigma^0_{gr} e^{-\delta B} + \sigma^0_{veg}\left(1 - e^{-\delta B}\right) \tag{6}$$

In Eq. (6), β has been replaced with δ to underline that the forest transmissivity is now expressed as function of biomass. The validity of the assumption that growing stock volume can simply be replaced with biomass will be discussed in Section 4.1.2.

3.2. Model training

Two of the three unknowns in the model in Eq. (6) are related to the backscatter from open ground not covered by vegetation (σ^0_{gr}) and to what is considered the backscatter from opaque forest canopies with infinite biomass (σ^0_{veg}). In Santoro et al. (2011) and Cartus et al. (2011), it was shown for C-band that the backscatter properties of open ground and dense forest canopies, and their temporal and spatial variations, could be identified with the aid of MODIS VCF by masking the intensity images for areas with low and high VCF canopy cover and taking the median of the measured intensities in the masked areas, respectively. In the case of open ground with low canopy cover, ancillary datasets were used to exclude land cover classes (settlements, industrial areas, water surfaces, etc.) for which the backscatter can differ substantially from that of open ground. In the case of the intensity observed over dense forests, denoted as σ^0_{df}, an additional compensation for residual backscatter contributions from the ground had to be carried out. The compensation of σ^0_{df} for residual ground contributions was accomplished with:

$$\sigma^0_{veg}(B_{df}) = \frac{\sigma^0_{df} - \sigma^0_{gr} e^{-\delta B_{df}}}{1 - e^{-\delta B_{df}}} \tag{7}$$

where B_{df} represents the biomass of dense forest. The estimation of σ^0_{veg} requires knowledge of δ and B_{df}, which means that some information about the biomass of dense forest in the particular region of interest is required (see Section 4.2).

3.3. Multi-temporal retrieval

Once the parameters have been estimated, the model can be inverted to estimate the biomass from the SAR data:

$$B = -\frac{1}{\delta} \ln\left(\frac{\sigma^0_{veg} - \sigma^0_{for}}{\sigma^0_{veg} - \sigma^0_{gr}}\right) \tag{8}$$

When inverting the model, some intensity measurements might in fact exceed the range of modeled intensities between σ^0_{gr} and σ^0_{veg}. Inversion for intensities lower than σ^0_{gr} would result in negative biomass estimates, which is why a biomass of 0 t/ha has to be assigned. In the case of high intensity values exceeding σ^0_{veg}, an inversion is not possible and for intensities slightly lower than σ^0_{veg}, the inversion could result in biomass estimates far exceeding the range of realistic biomass values, which is why a maximum biomass level, B_{max}, has to be defined up to which inversion is carried out (see Section 5). As was shown in Kurvonen et al. (1999), Rauste (2005) and Santoro et al. (2006, 2011) for C- and L-band intensity, the availability of multi-temporal stacks of data can help to improve the retrieval results. Since for the northeastern United States, at least partial multi-temporal PALSAR coverage was available, we adopted the approach used in Santoro et al. (2011), where a weighted combination of the biomass estimates from each image covering a particular pixel location, B_i, was computed to obtain new multi-temporal estimates, B_{mt}:

$$B_{mt} = \frac{\sum_{i=1}^{N} w_i B_i}{\sum_{i=1}^{N} w_i} \tag{9}$$

The weights, w_i, were calculated using the difference between σ^0_{veg} and σ^0_{gr}, referred to hereafter as the dynamic range. The larger the dynamic range, the more weight was given to the particular biomass estimate.

4. Analysis of the model training approach

4.1. Estimation of the forest transmissivity parameter δ

4.1.1. Regression analysis on δ

The forest transmissivity parameter δ in Eq. (6), which describes the trend of the backscatter with increasing biomass, cannot be estimated automatically. The backscatter trend can be expected to depend on the imaging conditions and the forest structural characteristics (Dobson et al., 1995; Lucas et al., 2010; Santoro et al., 2006). For the identification of plausible ranges of values, the model in Eq. (6) was first fitted to the observed relationship of ALOS PALSAR intensity and NBCD biomass by means of regression on a frame-by-frame basis for images from all mapping zones (see example in Fig. 2). For this, the ALOS and NBCD data were aggregated to 150 m pixel size to reduce the effect of noise on the parameter estimates (cf., Section 5.1). The obtained estimates for δ varied mostly in a narrow range between 0.005 and 0.01 ha/t (average of ~0.008 ha/t) for both polarizations with no apparent regional differences. In some cases, however, the estimates for HH intensity images reached very high values up to 0.03 ha/t. When looking at the goodness of the model fit in terms of the sum of squared residuals, it was found that the differences when using a fixed value for δ of 0.008 ha/t (an average value) or the particular value obtained from regression were marginal (<1%). These results suggested that the variations in the estimates for δ were to some degree

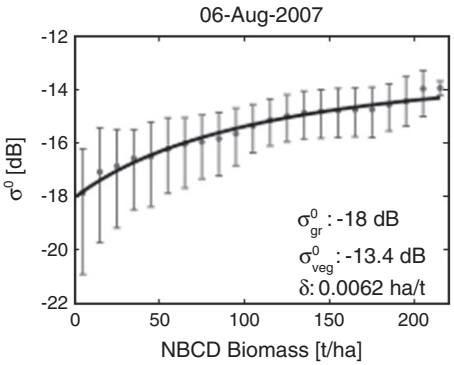

Fig. 2. L-HV intensity from 06-August-2007 as a function of NBCD biomass. The dots and vertical bars denote the mean and the range between the 10th and 90th percentiles of intensity for intervals of biomass, respectively. The curve presents the model in Eq. (6) fitted to the observations.

a consequence of the scatter in the relationship of L-band intensity and NBCD biomass. This assumption appeared to be confirmed by the observation that the extreme values ($\delta > 0.01$ ha/t) were obtained for images with low dynamic range (1–2 dB) and hence with a reduced sensitivity to biomass.

4.1.2. Compliance with the forest transmissivity concept in the model

In the model (Eqs. 3, 4), the forest transmissivity is considered a function of the canopy gap fraction and the canopy height. The forest transmissivity can also be expressed as a function of growing stock volume (Eq. (5)) because canopy cover and height are correlated to growing stock volume (Cartus et al., 2011; Santoro et al., 2002). The correlation of area-fill factor, canopy height and growing stock volume was illustrated in Santoro et al. (2002), where *in situ* measurements of growing stock volume, canopy height and estimates for the area-fill factor, derived from vertical photographs, were compared for a forest site in Sweden. In Cartus et al. (2011), a comparison of the VCF canopy cover map with inventory growing stock volume estimates for several forest sites in Central Siberia revealed a relationship similar to that of area-fill factor and growing stock volume shown in Santoro et al. (2002). For the modeling of L-band intensity as a function of aboveground biomass, we have so far assumed that a similar relationship existed between biomass and the area-fill factor. A comparison of the canopy cover estimates from MODIS VCF (year 2000) and the biomass estimates from NBCD in the Northeastern United States indicated the validity of this assumption. Fig. 3 illustrates for mapping zones 60 and 65 the relationship that closely resembles those presented in Santoro et al. (2002) and Cartus et al. (2011) for growing stock volume and area-fill factor/canopy cover. In analogy to Eqs. (4), (5), it should thus be possible to relate η to biomass through:

$$\eta = \frac{1 - e^{\delta B}}{1 - e^{\alpha h}} \tag{10}$$

The observed relationship between VCF canopy cover, assumed to represent η ($\times 100$), and biomass allowed us to investigate the physical reasonability of the values for δ, obtained in Section 4.1.1, by fitting Eq. (10) to the observations. For this, the canopy height was expressed as a function of biomass using an allometric equation that was derived from the FIA plot data and α was estimated by means of regression. The obtained curves describe well the relationship between VCF canopy cover and NBCD biomass when using values for δ between 0.005 and 0.01 ha/t (Fig. 3) and the corresponding estimates for α of 0.3 to 1 dB/m were highly plausible since values in a similar range have been reported from L-band attenuation experiments and model simulations (Chauhan et al., 1991; Kurum et al., 2009; Sheen et al., 1994; Shinohara et al., 1992; Ulaby et al., 1990). The use of higher values for δ (>0.01 ha/t) resulted in estimates for α that progressively exceeded the range of realistic values (e.g., ~1.5 dB/m for $\delta = 0.012$ ha/t; ~2 dB/m for $\delta = 0.014$ ha/t), which further confirmed our previous assumption that the extreme values for δ obtained in Section 4.1.1 were a consequence of the scatter in the relationship of L-band intensity and NBCD biomass. In summary, the results provided evidence for 1) the physical justification of the formulation of the Water-Cloud Model as function of aboveground biomass (Eqs. 6) and 2 the range of values for δ identified in Section 4.1.1.

4.1.3. Sensitivity of the biomass retrieval to δ

Given the objective of developing an automated retrieval algorithm, a scene-specific selection of δ is not feasible. In order to evaluate the effect of using a fixed value for δ on the retrieval performance, a sensitivity analysis was carried out by inverting the model using different values for δ (0.006–0.01 ha/t). Two scenarios were considered, one image with little sensitivity to biomass and one with high sensitivity (1 or 5 dB difference between σ^0_{gr} and σ^0_{df}). First, σ^0_{veg} was estimated using Eq. (7) (cf., Section 4.2) and then the model was inverted (Eq. 8). In both, the high and low sensitivity cases, the comparison of the biomass estimates revealed only a minor dependence on the particular value of δ in the biomass range that can be found in the northeastern US (Fig. 4). The sensitivity analysis thus suggested that the use of a fixed value for δ of 0.008 ha/t (i.e., an average value) for the biomass retrieval represented a justifiable compromise.

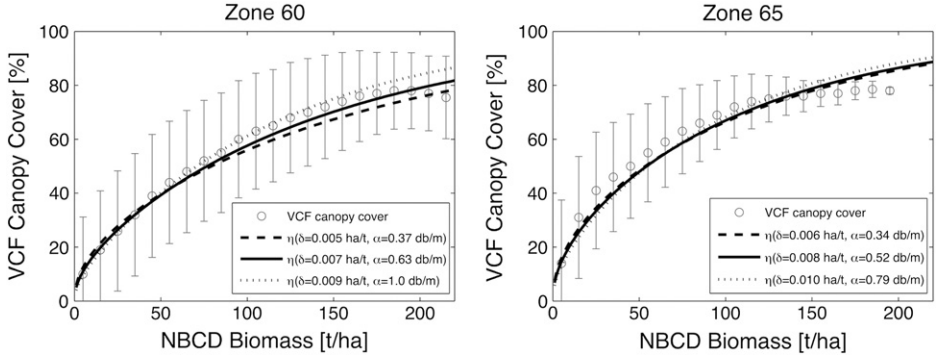

Fig. 3. Mean (circles) and standard deviation (vertical bars) of VCF canopy cover for intervals of NBCD biomass and modeled area-fill factor using Eq. (10) with different values for δ and the corresponding values for α obtained from regression. The canopy height was expressed as function of biomass using an allometric expression derived from the FIA plot data ($h = 1.04^* B^{0.57}$).

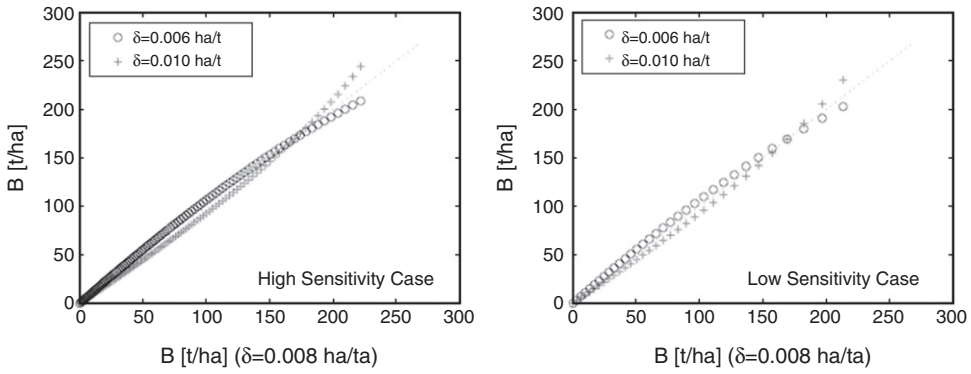

Fig. 4. Estimates for aboveground biomass (B) when using different values for the forest transmissivity parameter δ in Eq. (6) in the case of intensity images with high (left) and low (right) sensitivity to biomass.

4.2. Estimation of σ^0_{gr} and σ^0_{veg}

The dependence of the backscatter from open ground and forest canopies on the imaging conditions means that the backscatter signatures over forested terrain can change spatially and temporally. In Cartus et al. (2011), ERS-1/2 C-band backscatter and repeat-pass coherence properties of open ground and dense forests were inferred on a frame-by-frame basis (ERS frames covered an area of ~100 × 100 km^2) with the aid of the MODIS VCF canopy cover product. In Santoro et al. (2011), a spatially more adaptive approach was applied to identify the backscatter properties of open ground and forest canopies in ENVISAT ASAR C-band intensity on a pixel basis. Thresholds on VCF were used to delineate open ground and dense forest areas in the SAR intensity images in moving windows to estimate the parameters at pixel level. Since a certain number of open ground and dense forest pixels were required to obtain reliable parameter estimates (1–2% of the pixels in the estimation window), variable window sizes and VCF thresholds for the delineation of open ground (<15–30% canopy cover) and dense forest (>75% of maximum VCF canopy cover) pixels were used. The 90th percentile of the GSV distribution in the region covered by the particular intensity image (inferred from inventory data) was used to compensate σ^0_{df} for residual ground scattering contributions (Eq. 7).

We tested the adaptive model training approach for the ALOS PALSAR data using 1) the NLCD canopy density map for the delineation of open ground and dense forest, 2) the NLCD land cover map for the masking of water surfaces, cropland and developed areas and 3) the 90th percentile of FIA plot biomass in the region covered by the particular image as value for B_{df} to estimate σ^0_{veg} (Eq. 7). We found that due to the dense forestation of the study area, very large windows with side lengths in the range of 500 to 2000 pixels were required to obtain consistently at least 1% of ground pixels in the estimation windows. When using such large windows, the variations of the estimated parameters within the frames were mostly low; the standard deviation of σ^0_{gr} per image, for instance, was on average 0.15 dB. Because of the minor improvements in the algorithm performance that were to be expected from the adaptive training and the increased computational demands of a parameter estimation in moving windows, it was decided to switch back to a frame-by-frame training (i.e., σ^0_{gr} and σ^0_{veg} were estimated for entire intensity images). A sensitivity analysis with respect to 1) the NLCD canopy density thresholds used for the delineation of open ground and dense forest and 2) the percentile of the FIA plot biomass used for estimating B_{df} showed that no further adjustments to the model training procedure described in Santoro et al. (2011) were necessary.

5. Retrieval performance

For the assessment of the retrieval performance, model training and inversion were carried out for each of the 1310 intensity images (655 HH and 655 HV images). As with Santoro et al. (2011), a fixed biomass offset, ΔB, was used with respect to B_{df} to define the maximum retrievable biomass, B_{max} ($B_{max} = B_{df} + \Delta B$), when inverting the models to estimate the biomass (Eq. 8) for all pixels in the intensity images for which the NLCD land cover map reported forest. B_{max}

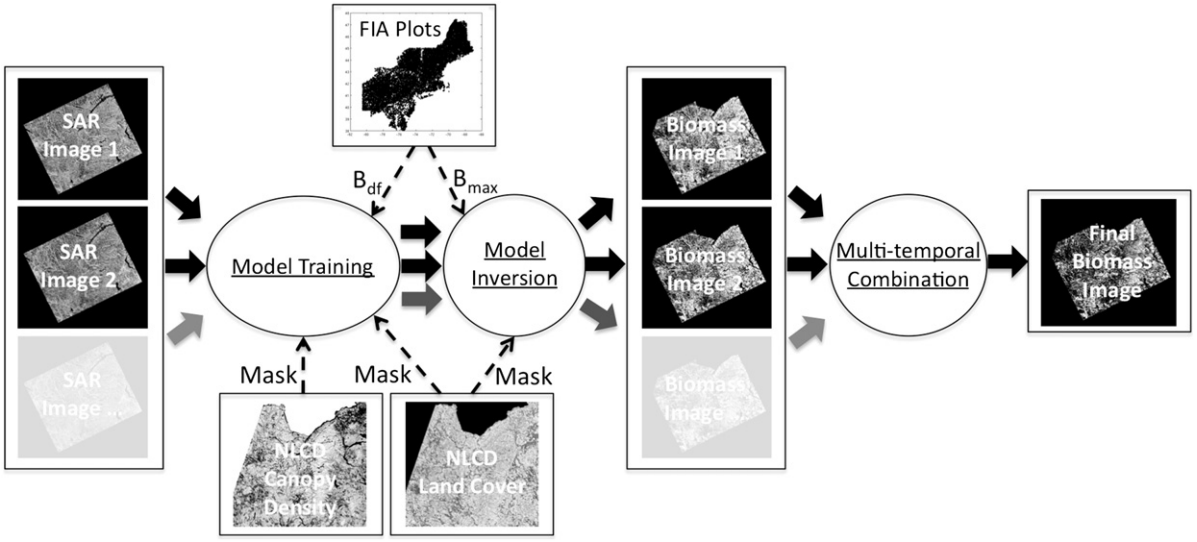

Fig. 5. Flowchart of the retrieval algorithm.

affects the retrieval results in the higher biomass ranges and therefore (primarily) derived population statistics such as county totals (cf., Santoro et al., 2011). That is why ΔB was adjusted so that the differences between the total biomass estimates per county and the FIA county-level estimates were minimized; this was the case when setting ΔB to 30 t/ha (see Section 5.3). The multi-temporal combination (Eq. 9) and mosaicking of the single image biomass maps were carried out in a single step for each of the six zones in the Northeastern US. Both, HH- as well as HV-intensity based biomass estimates were considered for the multi-temporal combination. A flowchart illustrating the final implementation of the retrieval algorithm has been provided in Fig. 5. A mosaic of the biomass maps for all six mapping zones is shown in Fig. 6.

5.1. Comparison with NBCD

In order to evaluate the retrieval performance, we compared the ALOS biomass maps to the NBCD maps. At this point, it is important to mention that a comparison of one remote sensing product (ALOS maps) against another (NBCD), even if validated, cannot be considered a comprehensive validation. Still, it is believed that such a comparison can provide valuable information about the possibility to depict the spatial distribution of aboveground biomass with ALOS PALSAR data. To account for potential forest cover changes, areas where the NLCD 2001/06 land cover maps indicated change were not considered. Changes in biomass between 2000 and 2007 due to tree growth and mortality were not compensated for. The average annual net growth rates in the northeastern US are in a range of 3 to 4 t/ha for young and below 2 t/ha for old stands (the growth rates were drawn from the FIA-based Carbon On Line Estimator: "http://www.ncasi2.org/COLE/").

The algorithm performance was assessed with the root mean square difference (RMSD) between the ALOS and NBCD maps calculated for each zone. At full resolution, the RMSDs were large (>80 t/ha). This might on one side have been a consequence of noise in the ALOS data (residual speckle, small scale environmental effects) but it also has to be considered that at the level of 30 m pixels, the NBCD map contains considerable uncertainty as well; note that the NBCD map was validated at segment (i.e., hectare) level. The comparison of the maps at 30 m pixel size was therefore of limited explanatory value. Hence, we repeated the comparison at different pixel aggregation scales between 150 m and 6 km. When aggregating the maps by means of simple block-averaging, the agreement increased substantially (Fig. 7, right). The largest improvement could be observed when aggregating up to ~1 km pixel size, for which the RMSD was in a range of 20 to 25 t/ha. In Fig. 7 (left), the ALOS biomass estimates for mapping zones 61 and 64 have been plotted against the NBCD biomass estimates for pixel sizes of 150 and 600 m. The comparison of the ALOS and NBCD biomass maps revealed a good agreement along the 1:1 line. The spread along the 1:1 line reduced substantially with increasing pixel size, which can be seen in Fig. 7 (left) from the decreasing length of the vertical bars. The ALOS biomass estimates, however, tended to be lower than the NBCD estimates when approaching a biomass of 200 t/ha, indicating saturation effects in the L-band data. The saturation effect could be observed for zones 60 to 64; in zones 65 and 66 the biomass hardly

Fig. 6. Aboveground forest biomass map for the northeastern United States produced from 655 ALOS PALSAR dual-polarization intensity images acquired in 2007/08.

reached 200 t/ha. The observed saturation effects at biomass levels somewhat below 200 t/ha could thus be expected to affect the biomass estimates for only a small proportion of the forests in the study area. In the FIA database, for instance, only about 2.5% of the plots in the northernmost states and 14% in the southernmost states in the study area reported a biomass of more than 180 t/ha.

5.2. Single-images and multi-temporal retrieval

To evaluate the importance of having multi-temporal stacks of L-band intensity, we first discuss the retrieval performance for single images. Fig. 8 shows for the L-band intensity images covering zone 64 the RMSD between the biomass estimates from single intensity images and NBCD as function of the dynamic range (at 150 m pixel size). The figure clearly shows that the dynamic range can be considered one of the main factors influencing the retrieval performance. The figure also shows that the RMSDs for HV intensity images tended to be lower (40–80 t/ha) than for HH intensity images (50–100 t/ha). For a given FBD HH and HV image pair, the RMSD was always lower for the HV image (5 to 10 t/ha). The differences in the dynamic ranges were most likely a consequence of differing imaging conditions. For the images covering New York State, we compared the dynamic ranges with the weather conditions at the time of the sensor overpasses. The comparison with the weather data revealed no correlation with temperature; note that the temperature was consistently above the freezing point for all images so that no major temperature related fluctuations of the dielectric properties of the trees were to be expected. Weak negative correlations were observed when relating the dynamic range to the total amount of rain in the days prior to the sensor overpasses. In both polarizations, there was a trend towards lower dynamic ranges with increasing amounts of precipitation (i.e., with increasing wetness of the soils and vegetation). The Pearson correlation coefficients were between −0.3 and −0.5 depending on which timeframe prior to the sensor overpasses was considered. This result is consistent with previous findings (Lucas et al., 2010; Salas et al., 2002).

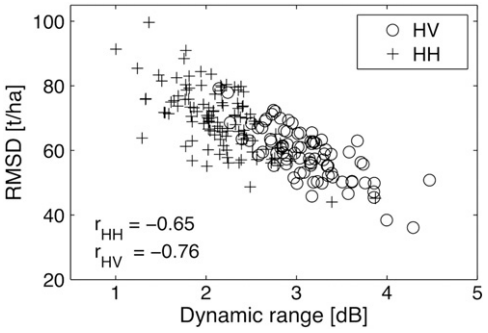

Fig. 8. RMSD between the biomass estimates from single HH (+) and HV (o) intensity images and NBCD as function of the dynamic range (zone 64, 150 m pixel size).

Fig. 9 illustrates the benefit of having multi-temporal data for an area where five FBD images were available. The dashed line shows the RMSD for each intensity image (HV: 55–59 t/ha, HH: 58–71 t/ha, 150 m pixel size), the solid line shows the change in RMSD when successively integrating the particular images into the multi-temporal retrieval. The multi-temporal combination resulted in a clear improvement of the RMSD when combining the available 5 HV images for about 10 t/ha (compared to the best HV image). When, in addition, integrating the corresponding HH images, only slight additional improvements of the RMSD for about 3 t/ha were achieved, which was not surprising since HV and HH intensity tend to be highly correlated when acquired simultaneously. These results confirmed that the multi-temporal combination allowed significant improvements of the biomass estimates. However, the improvements in terms of the RMSD of ~13 t/ha that were achieved with the multi-temporal combination were lower than the overall variability of the RMSD for single images (see Fig. 8). Considering both factors together, the variability of the retrieval performance for single images and the varying number of images in the multi-temporal stack, the observations in Figs. 8 and 9 suggested that the retrieval performance that was shown in Fig. 7 for entire mapping zones might not have been spatially consistent.

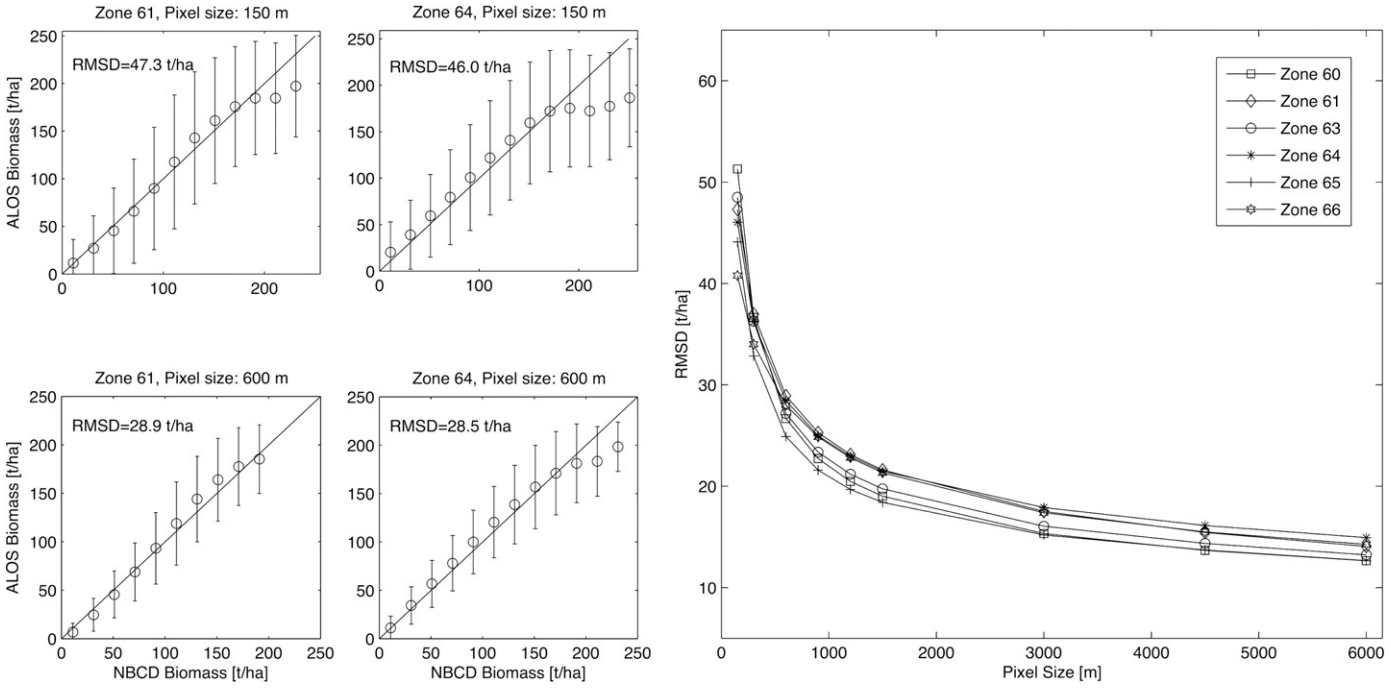

Fig. 7. Left: Average (circles) and standard deviation (vertical bars) of the multi-temporal ALOS biomass estimates for intervals of NBCD biomass at zones 61 and 64. Right: Root Mean Square Difference (RMSD) between the ALOS and NBCD biomass maps as a function of the pixel aggregation scale.

To assess the spatial consistency of the produced ALOS biomass maps (Fig. 6), the RMSD between the ALOS and NBCD biomass maps was analyzed with respect to the multi-temporal sum of weights (the denominator in Eq. 9) by calculating the RMSD separately for areas with a similar multi-temporal sum of weights (in 2 dB intervals). Across all mapping zones, we observed a clear decrease of the RMSD with increasing sum of weights up to about ~12 dB (see examples in Fig. 10). The decrease of the RMSD with increasing sum of weights showed that the number of images in the multi-temporal stack that would have been required to produce maps with spatially consistent accuracy depended on the properties of the images. Simply put, the more images that were acquired under adverse (e.g., rainy) conditions (causing lower dynamic ranges), the larger the multi-temporal stack needs to be. In the case of the PALSAR dataset available for the northeastern US, a multi-temporal sum of weights of about 12 dB was generally reached when four FBD acquisitions were available.

5.3. Comparison with FIA county statistics

The comparison of the ALOS biomass maps with NBCD indicated that, at least at aggregated scales, the spatial distribution of biomass could be depicted with the retrieval approach presented. To further assess the performance of the retrieval algorithm, we compared the ALOS biomass maps to FIA county-level total aboveground biomass statistics for 143 counties in Maine, New Hampshire, Vermont, Massachusetts, Rhode Island, Connecticut, New York and New Jersey. For the comparison of the ALOS and FIA estimates, the ALOS per-pixel (30×30 m^2) biomass estimates were summed per county. The comparison of the ALOS and FIA county-level estimates of total aboveground biomass resulted in a coefficient of determination (R^2) of 0.98 and a root mean square error (RMSE) of 2.75 10^6 t. When calculating the average biomass per county (i.e., the total biomass divided by the county size in hectares), the RMSE was 12.9 t/ha and the R^2 was 0.86 (Fig. 11). The FIA county statistics included information about the sampling error, which could be used to approximate the confidence intervals of the FIA estimates (cf., Bechtold and Patterson, 2005). The sampling error was between 2% and 110% for the largest counties (with the largest number of sample plots) and for the smallest counties, respectively; the size of the counties ranged from 64 to 17686 km^2. As can be seen in Fig. 12, the ALOS total aboveground biomass estimates were within the 95% confidence intervals of the FIA estimates for most (92%) of the 143 counties.

The main parameter in the retrieval algorithm that had an influence on the derived population estimates was the maximum retrievable biomass, B_{max}. When increasing or decreasing B_{max} in steps of 10 t/ha, the estimated total biomass per county increased or decreased for about 2% to 3% at all counties, respectively. When considering the entire study area, the best results (in terms of the RMSE and the number of counties for which the ALOS biomass estimates were within the 95% confidence intervals of the FIA estimates) were achieved when setting ΔB to 30 t/ha (i.e., $B_{max} = B_{df} + 30$ t/ha). At the level of states, however, the agreement of the ALOS and FIA total biomass estimates could have been somewhat improved (2% to 15% lower RMSE) by adjusting ΔB. In the case of Maine and New Hampshire, for instance, the optimal value for ΔB would have been 20 t/ha. In the case of Vermont, Connecticut and Massachusetts, instead, the optimal value for ΔB would have been in the range of 40 to 50 t/ha. Keeping in mind, however, that the retrieval algorithm aims at large areas, the definition of the maximum retrievable biomass with a fixed biomass offset with respect to B_{df} appeared to be appropriate.

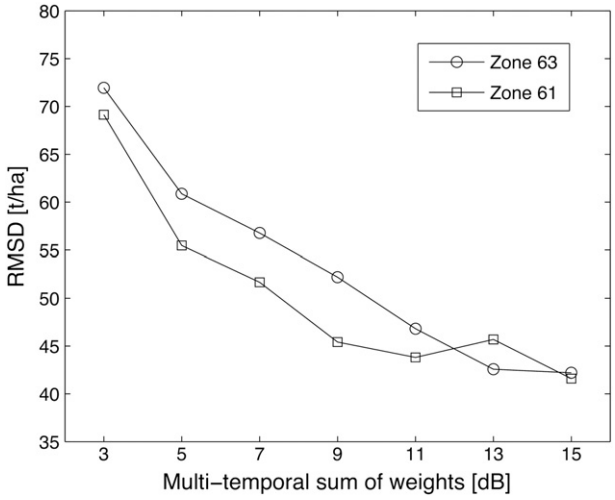

Fig. 10. RMSD between the ALOS and NBCD biomass maps (at 150 m pixel size) as a function of the multi-temporal sum of weights (denominator in Eq. 9).

6. Conclusions

In this paper we investigated the potential to retrieve forest aboveground biomass from ALOS PALSAR dual-polarization intensity data in the northeastern United States. As with Santoro et al. (2011) and Cartus et al. (2011), we accomplished the fully-automated training of a Water-Cloud type of model, adapted to describe L-band backscatter in co- and cross-polarization as a function of aboveground

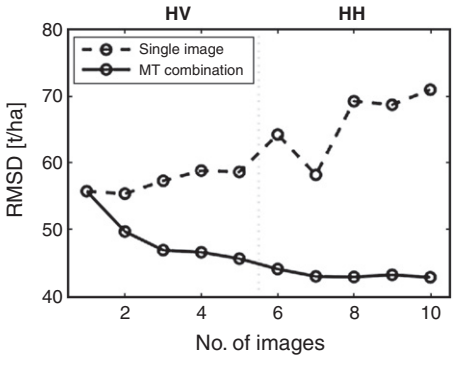

Fig. 9. Effect of the multi-temporal combination on the agreement of the ALOS and NBCD biomass maps (at 150 m pixel size). The circles connected by the dashed line denote the RMSD for each image and those connected by the solid line show how the RMSD changed when successively integrating the single image estimates into the multi-temporal retrieval.

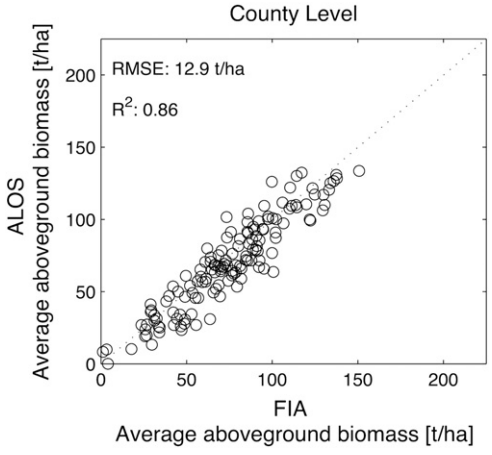

Fig. 11. Average aboveground biomass according to the ALOS biomass map and FIA biomass statistics for 143 counties in the Northeastern United States.

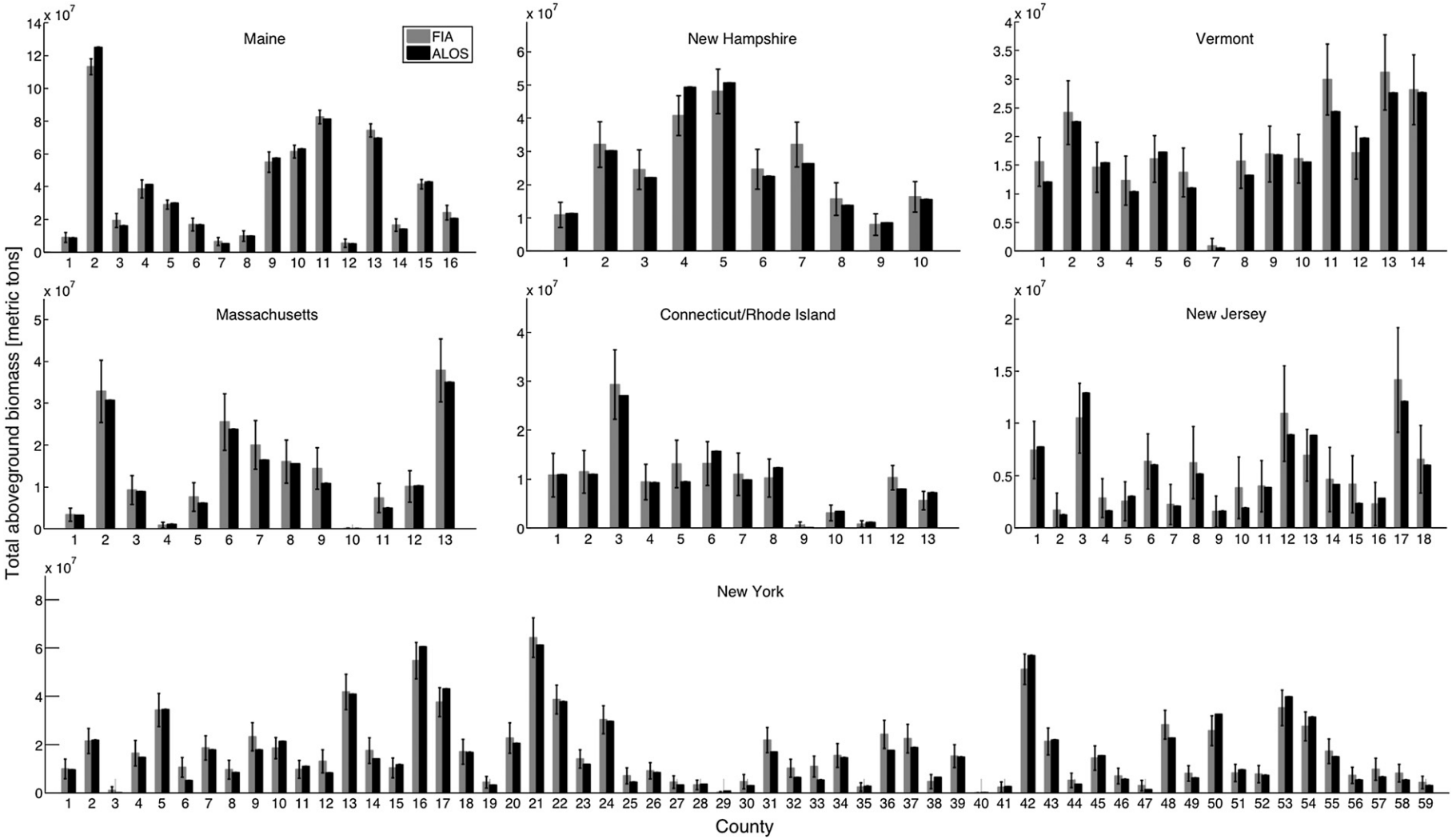

Fig. 12. Comparison of FIA and ALOS total aboveground biomass estimates per county for eight states in the Northeastern USA. The vertical lines denote the 95% confidence intervals of the FIA estimates.

biomass, using an optical remote sensing product, the NLCD canopy density map. Large-area retrieval was tested for an ALOS PALSAR dataset comprising 655 HH and HV intensity images to map forest aboveground biomass in the northeastern United States using a multi-temporal retrieval approach where the biomass estimates for each image in a multi-temporal stack were combined in a weighted manner. A comparison with the National Biomass and Carbon Dataset 2000 indicated strong agreement when aggregating the original 30 m maps to coarser pixel sizes (>500 m). A comparison against FIA biomass statistics confirmed that at aggregated scales (i.e., county level) the approach produced accurate biomass estimates. Nevertheless, the investigation revealed clear limitations, which were related to 1) the lack of a consistent multi-temporal coverage of ALOS PALSAR dual-polarization data and 2) the dependence of the single image retrieval on the imaging conditions. Both factors combined were found to entail spatially inconsistent retrieval accuracies in the ALOS biomass maps. In addition, we observed saturation effects at biomass levels somewhat below 200 t/ha, which is, however, higher than that observed in previous studies.

The results indicate that with the approach presented the achieved accuracies are not likely high enough for applications in silvicultural planning. Nevertheless, the maps may still provide valuable information for various purposes and interest groups. As was discussed in Tomppo et al. (2008) for the Landsat-based kNN growing stock volume and biomass maps that have been produced for Sweden and Finland with similar constraints concerning the retrieval accuracy at pixel or stand level, potential use could be in landscape ecology and nature protection, NFI sampling simulation or administrative planning. At larger scales, the retrieval approach presented here might allow for the generation of useful information for the calibration and validation of terrestrial biosphere models (Le Toan et al., 2004), which work at rather coarse spatial scales (typically at 0.1–0.5° grids), or complement national and international carbon stock mapping and reporting efforts, in particular for areas with limited field data.

Acknowledgements

The work presented in this paper was carried out with support from the USDA project “Towards Spatially Explicit Quantification of Carbon Flux (2000–2007) in Northeastern U.S. Forests Linking Remote Sensing with Forest Inventory Data” (project number: MASR-2008-01311).

References

Askne, J. I. H., Dammert, P. B. G., Ulander, L. M. H., & Smith, G. (1997). C-band repeat-pass interferometric SAR observations of the forest. *IEEE Transactions on Geoscience and Remote Sensing*, *35*(1), 25–35.

Askne, J. I. H., Santoro, M., Smith, G., & Fransson, J. E. S. (2003). Multitemporal repeat-pass SAR interferometry of boreal forests. *IEEE Transactions on Geoscience and Remote Sensing*, *41*(7), 1540–1550.

Attema, E. P. W., & Ulaby, F. T. (1978). Vegetation modeled as a water cloud. *Radio Science*, *13*, 357–364.

Baccini, A., Laporte, N. T., Goetz, S. J., Sun, M., & Dong, H. (2008). A first map of tropical Africa's above-ground biomass derived from satellite imagery. *Environmental Research Letters*, *3* (9 pp.).

Bailey, R. G. (1995). Description of the ecoregions of the United States. *Miscellaneous publication no. 1391* (2nd ed.). Washington, DC: U.S. Department of Agriculture Forest Service (108 pp.).

Baker, J., & Luckman, A. (1999). Microwave observations of boreal forests in the NOPEX area of Sweden and a comparison with observations of a temperate plantation in the United Kingdom. *Agricultural and Forest Meteorology*, *98–99*, 389–416.

Balzter, H., Baker, J., Hallikainen, M. T., & Tomppo, E. (2002). Retrieval of timber volume and snow water equivalent over a Finnish boreal forest from airborne polarimetric Synthetic Aperture Radar. *International Journal of Remote Sensing*, *23*(16), 3185–3208.

Bechtold, W. A., & Patterson, P. L. (Eds.). (2005). *The enhanced forest inventory and analysis program—National sampling design and estimation procedures. General Technical Report GTR-SRS-080*. Asheville, NC: U.S. Department of Agriculture, Forest Service, Southern Research Station (85 pp.).

Blackard, J., Finco, M., Helmer, E., Holden, G., Hoppus, M., Jacobs, D., et al. (2008). Mapping U.S. forest biomass using nationwide forest inventory data and moderate resolution information. *Remote Sensing of Environment*, *112*(4), 1658–1677.

Boudreau, J., Nelson, R., Margolis, H., Beaudoin, A., Guindon, L., & Kimes, D. (2008). Regional aboveground forest biomass using airborne and spaceborne LiDAR in Québec. *Remote Sensing of Environment*, *112*(10), 3876–3890.

Cartus, O., Santoro, M., Schmullius, C. C., & Li, Z. (2011). Large area forest stem volume mapping in the boreal zone using synergy of ERS-1/2 tandem coherence and MODIS vegetation continuous fields. *Remote Sensing of Environment*, *115*, 931–943.

Castel, T., Beaudoin, A., Stach, N., Stussi, N., Le Toan, T., & Durand, P. (2001). Sensitivity of space-borne SAR data to forest parameters over sloping terrain. Theory and experiment. *International Journal of Remote Sensing*, *22*(12), 2351–2376.

Chauhan, N. S., Lang, R., & Ranson, K. J. (1991). Radar modeling of a boreal forest. *IEEE Transactions on Geoscience and Remote Sensing*, *29*(4), 627–638.

Dobson, M. C., Ulaby, F. T., Le Toan, T., Beaudoin, A., Kasischke, E. S., & Christensen, N. (1992). Dependence of radar backscatter on coniferous forest biomass. *IEEE Transactions on Geoscience and Remote Sensing*, *30*(2), 412–415.

Dobson, M. C., Ulaby, F. T., Pierce, L. E., Sharik, T., Bergen, K., Kellndorfer, J. M., et al. (1995). Estimation of forest biophysical characteristics in Northern Michigan with SIR-C/X-SAR. *IEEE Transactions on Geoscience and Remote Sensing*, *33*(4), 877–895.

Fransson, J. E. S., & Israelsson, H. (1999). Estimation of stem volume in boreal forests using ERS-1 C- and JERS-1 L-band SAR data. *International Journal of Remote Sensing*, *20*(1), 123–137.

Gesch, D., Oimoen, M., Greenlee, S., Nelson, C., Steuck, M., & Tyler, D. (2002). The national elevation dataset. *Photogrammetric Engineering and Remote Sensing*, *68*, 5–11.

Goetz, S. J., Baccini, A., Laporte, N. T., Johns, T., Walker, W., Kellndorfer, J. M., et al. (2009). Mapping and monitoring carbon stocks with satellite observations: A comparison of methods. *Carbon balance and management*, *4*(2).

Hajnsek, I., Kugler, F., Lee, S. K., & Papathanassiou, K. P. (2009). Tropical-forest-parameter estimation by means of Pol-InSAR: The INDREX-II campaign. *IEEE Transactions on Geoscience and Remote Sensing*, *47*(2), 481–493.

Hansen, M. C., DeFries, R. S., Townshend, J. R. G., Carroll, M., Dimiceli, C., & Sohlberg, R. A. (2003). Global percent tree cover at a spatial resolution of 500 Meters: First results of the MODIS vegetation continuous fields algorithm. *Earth Interactions*, *7*(10), 1–15.

Harrell, P., Bourgeau-Chavez, L. L., Kasischke, E. S., French, N. H. F., & Christensen, N. L. (1995). Sensitivity of ERS-1 and JERS-1 radar data to biomass and stand structure in Alaskan boreal forest. *Remote Sensing of Environment*, *54*(3), 247–260.

Harrell, P., Kasischke, E. S., Bourgeau-Chavez, L. L., Haney, E., & Christensen, N. L. (1997). Evaluation of approaches to estimating aboveground biomass in Southern pine forests using SIR-C data. *Remote Sensing of Environment*, *59*(2), 223–233.

Hoekman, D., & Quinones, M. J. (2000). Land cover type and biomass classification using AirSAR data for evaluation of monitoring scenarios in the Colombian Amazon. *IEEE Transactions on Geoscience and Remote Sensing*, *38*(2), 685–696.

Holecz, F., Meier, E., Piesbergen, J., Nüesch, D., & Moreira, J. (1994). Rigorous derivation of backscattering coefficient. *IEEE Geoscience and Remote Sensing Society Newsletter*, *92*, 6–14.

Homer, C., Dewitz, J., Fry, J., Coan, M., Hossain, N., Larson, C., et al. (2007). Completion of the 2001 National Land Cover Database for the Conterminous United States. *Photogrammetric Engineering and Remote Sensing*, 337–341 (April 2007).

Houghton, R. A. (2005). Aboveground forest biomass and the global carbon balance. *Global Change Biology*, *11*(6), 945–958.

Hyyppä, J. M., Hyyppä, H. J., Inkinen, M., & Engdahl, M. E. (2000). Accuracy comparison of various remote sensing data sources in the retrieval of forest stand attributes. *Forest Ecology and Management*, *128*, 109–120.

Imhoff, M. (1995). Radar backscatter and biomass saturation: Ramifications for global biomass inventory. *IEEE Transactions on Geoscience and Remote Sensing*, *33*(2), 511–518.

IPCC (2006). *IPCC guidelines for National Greenhouse Gas Inventories*. Japan: Institute for Global Environmental Strategies.

Jenkins, J. C., Chojnacky, D. C., Heath, L. S., & Birdsey, R. A. (2003). National-scale biomass estimators for United States tree species. *Forest Science*, *49*(1), 12–35.

Karam, M., Amar, F., Fung, A. K., Mougin, E., Lopes, A., Le Vine, D. M., et al. (1995). A microwave polarimetric scattering model for forest canopies based on vector radiative transfer theory. *Remote Sensing of Environment*, *53*, 16–30.

Karam, M., Fung, A. K., Lang, R. H., & Chauhan, N. S. (1992). A microwave scattering model for layered vegetation. *IEEE Transactions on Geoscience and Remote Sensing*, *30*, 767–784.

Kasischke, E. S., Tanase, M., Bourgeau-Chavez, L. L., & Borr, M. (2011). Soil moisture limitations on monitoring boreal forest regrowth using spaceborne L-band SAR data. *Remote Sensing of Environment*, *115*(1), 227–232.

Kellndorfer, J. M., Dobson, M. C., Vona, J. D., & Clutter, M. (2003). Toward precision forestry: Plot-level parameter retrieval for slash pine plantations with JPL AIRSAR. *IEEE Transactions on Geoscience and Remote Sensing*, *41*(7), 1571–1582.

Kellndorfer, J. M., Walker, W. S., Kirsch, K., Fiske, G., Bishop, J., LaPoint, E., Hoppus, M., & Westfall, J. (in preparation). Development of a U.S. National Biomass and Carbon Dataset for the year 2000 through exploitation of InSAR and optical remote sensing. *Remote Sensing of Environment*.

Kellndorfer, J. M., Walker, W., LaPoint, E., Hoppus, M., & Westfall, J. (2006). Modeling height, biomass, and carbon in U.S. Forests from FIA, SRTM, and Ancillary National Scale Data Sets. *IEEE International Symposium on Geoscience and Remote Sensing'06, July 31st - August 4th, Denver, USA* (pp. 3591–3594).

Kellndorfer, J. M., Walker, W., Pierce, L. E., Dobson, M. C., Fites, J., Hunsaker, C., et al. (2004). Vegetation height estimation from Shuttle Radar Topography Mission and National Elevation Datasets. *Remote Sensing of Environment*, *93*(3), 339–358.

Kurum, M., Lang, R. H., O'Neill, P. E., Joseph, A. T., Jackson, T. J., & Cosh, M. H. (2009). L-band radar estimation of forest attenuation for active/passive soil moisture inversion. *IEEE Transactions on Geoscience and Remote Sensing*, *47*(9), 3026–3040.

Kurvonen, L., Pulliainen, J. T., & Hallikainen, M. T. (1999). Retrieval of biomass in boreal forests from multitemporal ERS-1 and JERS-1 SAR images. *IEEE Transactions on Geoscience and Remote Sensing*, *37*(1), 198–205.

Kwok, R., Rignot, E., Way, J., Freeman, A., & Holt, J. (1994). Polarization signatures of frozen and thawed forests of varying environmental state. *IEEE Transactions on Geoscience and Remote Sensing*, *32*(2), 371–381.

Le Toan, T., Beaudoin, A., Riom, J., & Guyon, D. (1992). Relating forest biomass to SAR data. *IEEE Transactions on Geoscience and Remote Sensing*, *30*(2), 403–411.

Le Toan, T., Quegan, S., Woodward, I., Lomas, M., Delbart, N., & Picard, G. (2004). Relating radar remote sensing of biomass to modelling of forest carbon budgets. *Climatic Change*, *67*, 379–402.

Lefsky, M. A. (2010). A global forest canopy height map from the Moderate Resolution Imaging Spectroradiometer and the Geoscience Laser Altimeter System. *Geophysical Research Letters*, *37*(15), 1–5.

Lopes, A., Nezry, E., Touzi, R., & Laur, H. (1993). Structure detection and statistical adaptive speckle filtering in SAR images. *International Journal of Remote Sensing*, *14*, 1735–1758.

Lucas, R. M., Armston, J., Fairfax, R., Fensham, R., Accad, A., Carreiras, J., et al. (2010). An evaluation of the ALOS PALSAR L-band backscatter—above ground biomass relationship Queensland, Australia: Impacts of surface moisture condition and vegetation structure. *IEEE Journal of Selected Topics in Applied Earth Observations and Remote Sensing*, *3*(4), 576–593.

Lucas, R. M., Cronin, N., Lee, A., Moghaddam, M., Witte, C., & Tickle, P. (2006). Empirical relationships between AIRSAR backscatter and LiDAR-derived forest biomass, Queensland, Australia. *Remote Sensing of Environment*, *100*(3), 407–425.

Luckman, A., Baker, J., Kuplich, T. M., Da Costa Freitas Yanasse, C., & Frery, A. C. (1997). A study of the relationship between radar backscatter and regenerating tropical forest biomass for spaceborne SAR instruments. *Remote Sensing of Environment*, *60*(1), 1–13.

Mitchard, E. T. A., Saatchi, S. S., Woodhouse, I. H., Nangendo, G., Ribeiro, N. S., Williams, M., et al. (2009). Using satellite radar backscatter to predict above-ground woody biomass: A consistent relationship across four different African landscapes. *Geophysical Research Letters*, *36*(23), 1–6.

Myneni, R. B., Dong, J., Tucker, C. J., Kaufmann, R. K., Kauppi, P. E., Liski, J., et al. (2001). A large carbon sink in the woody biomass of Northern forests. *Proceedings of the National Academy of Sciences of the United States of America*, *98*(26), 14784–14789.

Nelson, R., Ranson, K. J., Sun, G., Kimes, D., Kharuk, V., & Montesano, P. M. (2009). Estimating Siberian timber volume using MODIS and ICESat/GLAS. *Remote Sensing of Environment*, *113*(3), 691–701.

Neumann, M., Ferro-Famil, L., & Reigber, A. (2010). Estimation of forest structure, ground, and canopy layer characteristics from multibaseline polarimetric interferometric SAR data. *IEEE Transactions on Geoscience and Remote Sensing*, *48*(3), 1086–1104.

Papathanassiou, K. P., & Cloude, S. R. (2001). Single-baseline polarimetric SAR interferometry. *IEEE Transactions on Geoscience and Remote Sensing*, *39*(11), 2352–2363.

Picard, G., Le Toan, T., Quegan, S., Caraglio, Y., & Castel, T. (2004). Radiative transfer modeling of cross-polarized backscatter from a pine forest using the discrete ordinate and eigenvalue method. *IEEE Transactions on Geoscience and Remote Sensing*, *42*(8), 1720–1730.

Pierce, L. E., Bergen, K., Dobson, M. C., & Ulaby, F. T. (1998). Multitemporal land-cover classification using SIR-C/X-SAR Imagery. *Remote Sensing of Environment*, *64*, 20–33.

Pulliainen, J. T., Heiska, K., Hyyppä, J. M., & Hallikainen, M. T. (1994). Backscattering properties of boreal forests at the. *IEEE Transactions on Geoscience and Remote Sensing*, *32*(5), 1041–1050.

Pulliainen, J. T., Kurvonen, L., & Hallikainen, M. T. (1999). Multitemporal behavior of L- and C-band SAR observations of boreal forests. *IEEE Transactions on Geoscience and Remote Sensing*, *37*(2), 927–937.

Ranson, K. J., Saatchi, S. S., & Sun, G. (1995). Boreal forest ecosystem characterization with SIR-C/XSAR. *IEEE Transactions on Geoscience and Remote Sensing*, *33*, 867–876.

Ranson, K. J., & Sun, G. (1994). Mapping biomass of a northern forest using multifrequency SAR data. *IEEE Transactions on Geoscience and Remote Sensing*, *32*(2), 388–396.

Ranson, K. J., & Sun, G. (2000). Effects of environmental conditions on boreal forest classification and biomass estimates with SAR. *IEEE Transactions on Geoscience and Remote Sensing*, *38*(3), 1242–1252.

Rauste, Y. (2005). Multi-temporal JERS SAR data in boreal forest biomass mapping. *Remote Sensing of Environment*, *97*, 263–275.

Reese, H., Nilsson, M., Pahén, T. G., Hagner, O., Joyce, S., Tingelöf, U., et al. (2003). Countrywide estimates of forest variables using satellite data and field data from the National Forest Inventory. *Ambio*, *32*(8), 542–548.

Rignot, E., Way, J., Williams, C., & Viereck, L. (1994a). Radar estimates of aboveground biomass in boreal forests of interior Alaska. *IEEE Transactions on Geoscience and Remote Sensing*, *32*(5), 1117–1124.

Rignot, E., Williams, C. L., Way, J., & Viereck, L. (1994b). Mapping of forest types in Alaskan boreal forests using SAR imagery. *IEEE Transactions on Geoscience and Remote Sensing*, *32*(5), 1051–1059.

Rosenqvist, A., Shimada, M., Ito, N., & Watanabe, M. (2007). ALOS PALSAR: A pathfinder mission for global-scale monitoring of the environment. *IEEE Transactions on Geoscience and Remote Sensing*, *45*(11), 3307–3316.

Ruesch, A., & Gibbs, H. K. (2008). *New IPCC Tier-1 global biomass carbon map for the year 2000*. Oak Ridge, TN: Carbon Dioxide Information Analysis Center, Oak Ridge National Laboratory.

Saatchi, S., Houghton, R., Avala, R., Yu, Y., & Soares, J. V. (2007). Spatial distribution of live aboveground biomass in Amazon basin. *Global Change Biology*, *13*, 816–837.

Saatchi, S. S., Marlier, M., Chazdon, R. L., Clark, D. B., & Russell, A. E. (2011). Impact of spatial variability of tropical forest structure on radar estimation of aboveground biomass. *Remote Sensing of Environment*, *115*(11), 2836–2849.

Saatchi, S. S., & Moghaddam, M. (2000). Estimation of crown and stem water content and biomass of boreal forest using polarimetric SAR imagery. *IEEE Transactions on Geoscience and Remote Sensing*, *38*(2), 697–709.

Salas, W., Ducey, M. J., Rignot, E., & Skole, D. (2002). Assessment of JERS-1 SAR for monitoring secondary vegetation in Amazonia: I. Spatial and temporal variability in backscatter across a chrono-sequence of secondary vegetation stands in Rondonia. *International Journal of Remote Sensing*, *23*(7), 1357–1379.

Sandberg, G., Ulander, L. M. H., Fransson, J. E. S., Holmgren, J., & Le Toan, T. (2011). L- and P-band backscatter intensity for biomass retrieval in hemiboreal forest. *Remote Sensing of Environment*, *115*(11), 2874–2886.

Santoro, M., Askne, J. I. H., Smith, G., & Fransson, J. E. S. (2002). Stem volume retrieval in boreal forests from ERS-1/2 interferometry. *Remote Sensing of Environment*, *81*(1), 19–35.

Santoro, M., Beer, C., Cartus, O., Schmullius, C. C., Shvidenko, A., McCallum, I., et al. (2011). Retrieval of growing stock volume in boreal forest using hyper-temporal series of Envisat ASAR ScanSAR backscatter measurements. *Remote Sensing of Environment*, *115*(2), 490–507.

Santoro, M., Eriksson, L. E. B., Askne, J. I. H., & Schmullius, C. C. (2006). Assessment of stand-wise stem volume retrieval in boreal forest from JERS-1 L-band SAR backscatter. *International Journal of Remote Sensing*, *27*(16), 3425–3454.

Santoro, M., Fransson, J. E. S., Eriksson, L. E. B., Magnusson, M., Ulander, L. M. H., & Olsson, H. (2009). Signatures of ALOS PALSAR L-Band Backscatter in Swedish Forest. *IEEE Transactions on Geoscience and Remote Sensing*, *47*(12), 4001–4019.

Sheen, D. R., Malinas, N. P., Kletzli, D. W., Lewis, T. B., & Roman, J. F. (1994). Foliage transmission measurements using a SAR system. *IEEE Transactions on Geoscience and Remote Sensing*, *32*(1), 118–130.

Shimada, M., Isoguchi, O., Tadono, T., & Isono, K. (2009). PALSAR radiometric and geometric calibration. *IEEE Transactions on Geoscience and Remote Sensing*, *47*(12), 3915–3932.

Shinohara, H., Homma, T., Nohmi, H., Hirosawa, H., & Tagawa, T. (1992). Relation between L-band microwave penetration/backscattering characteristics and state of trees. *IEEE International Geoscience and Remote Sensing Symposium '92, May 26th - 29th, Houston, USA* (pp. 539–541).

Skriver, H., Mortensen, H. B., & Gudmandsen, P. (1994). Calibration and modelling of MAESTRO 1 polarimetric SAR data of a forest area in Les Landes, France. *International Journal of Remote Sensing*, *15*(14), 2737–2754.

Thiel, C. J., Thiel, C., & Schmullius, C. C. (2009). Operational large-area forest monitoring in Siberia using ALOS PALSAR summer intensities and winter coherence. *IEEE Transactions on Geoscience and Remote Sensing*, *47*, 3993–4000.

Tomppo, E., Olsson, H., Stahl, G., Nilsson, M., Hagner, O., & Katila, M. (2008). Combining national forest inventory field plots and remote sensing data for forest databases. *Remote Sensing of Environment*, *112*(5), 1982–1999.

Ulaby, F. T., Whitt, M. W., & Dobson, M. C. (1990). Measuring the propagation properties of a forest canopy using a polarimetric scatterometer. *IEEE Transactions on Antennas and Propagation*, *38*(2), 251–258.

Wagner, W., Luckman, A., Vietmeier, J., Tansey, K. J., Balzter, H., Schmullius, C. C., et al. (2003). Large-scale mapping of boreal forest in SIBERIA using ERS tandem coherence and JERS backscatter data. *Remote Sensing of Environment*, *85*, 125–144.

Walker, W., Kellndorfer, J. M., Lapoint, E., Hoppus, M., & Westfall, J. (2007). An empirical InSAR-optical fusion approach to mapping vegetation canopy height. *Remote Sensing of Environment*, *109*(4), 482–499.

Wang, Y., Paris, J. F., & Davis, F. W. (1998). Inclusion of a simple multiple scattering model into a microwave canopy backscatter model. *Remote Sensing of Environment*, *63*, 101–111.

Way, J., Rignot, E., McDonald, K. C., Oren, R., Kwok, R., Bonan, G., et al. (1994). Evaluating the type and state of Alaska taiga forests with imaging radar for use in ecosystem models. *IEEE Transactions on Geoscience and Remote Sensing*, *32*(2), 353–370.